JOURNAL OF MATERIALS SCIENCE 30 (1995) 2747–2758

Comparison of beginning and ending microstructures in metal shaped charges as a means to explore mechanisms for plastic deformation at high rates

L. E. MURR, C.-S. NIOU, J. C. SANCHEZ, H. K. SHIH, L. DUPLESSIS, S. PAPPU
Department of Metallurgical and Materials Engineering and Materials Research Institute, The University of Texas at El Paso, El Paso, TX 79968, USA

L. ZERNOW
Zernow Technical Services, Inc., San Dimas, CA 91773, USA

Optical metallography and transmission electron microscopy (TEM) observations were made of a variety of forged or sputtered copper, molybdenum, and tantalum shaped charge components. The beginning shaped charge liner grain sizes and sub-structures were compared with those observed in residual (ending), recovered and corresponding jet fragments and slugs. The wide range of microstructures and evolutionary features of observed microstructures can be characterized by low-energy dislocation structure (LEDS) principles which are altered because the shaped charge deformation corresponds to hot working, and dynamic recovery and recrystallization play a prominent role. There is a prominent relationship between the starting liner grain size, D_0, and the ratio D_0/D_s, where D_s is the ending (slug or jet), steady-state grain size. As a consequence of this relationship, it appears that the volumetric stored energy, which depends upon the grain size and dislocation density (or degree of deformation), is the critical issue in controlling shaped charge jet stability.

1. Introduction

The conical metal shaped charge or lined cavity explosive charge represents a novel and practical example of extreme plastic deformation involving hypervelocity forming rates. As illustrated schematically in Fig. 1, a shaped charge employing a conical metal liner uses a high explosive to create a shock wave at pressures approaching 100 GPa, which collapses the metal cone to form a stretching (and penetrating) jet of metal approximately 1/20 of the cone diameter. This jet, which is strained about 1000% at strain rates in excess of $10^6\ s^{-1}$, forms from roughly the inner 1/5th of the cone wall thickness (Fig. 1) while the remaining liner mass flows plastically into a slug which is accelerated along the charge axis at a slower velocity than the jet, and at the tail of the jet. The penetration of the shaped charge jet into metal targets is proportional to $(\rho_p/\rho_t)^{\frac{1}{2}}$ (where ρ_p is the jet density and ρ_t is the target density) and is also significantly influenced by the stand-off distance (measured in cone diameters (CD)) from the target surface. Penetration is also influenced by the jet stability or the length of time the jet remains unparticulated. That is, as the jet in Fig. 1 is stretched as a consequence of the velocity gradient created along the charge axis, periodic necking will occur [1] and the elongated jet will particulate into necked fragments.

Duffy and Golaski [2] recently demonstrated that the jet stability and penetration of standard copper shaped charges having 81 mm diameter liner cones were markedly influenced by varying the starting liner grain size in a range of roughly 20–120 μm. The penetration into RHA (rolled homogeneous armour) plate was increased by approximately 20% for the smallest grain sizes, and pointed up the fact that even in this extreme deformation regime, plastic flow was observably influenced by variations in the grain size of the starting liner cone.

In more recent observations of recovered jet fragments and slugs, Gurevitch *et al.* [3] and Murr *et al.* [4, 5] have observed that the jet fragment and slug microstructures for copper and tantalum shaped charges were significantly altered from the starting liner microstructures, and variations in starting tantalum liner grain structure and microstructure had a noticeable effect on the residual jet and slug microstructures. More specifically, for starting liner grain sizes of 35–60 μm, the smallest grain sizes in the recovered jet fragments and slugs were always smaller, often as much as 10^2 smaller. These observations were interpreted to be indicative of the fact that dynamic recovery and recrystallization played a significant role in the deformation process, especially since the associated process temperatures were considered to be

0022–2461

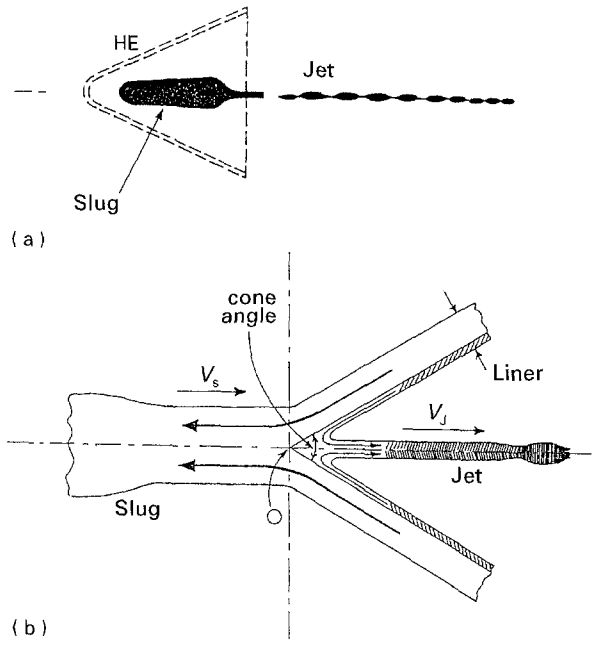

Figure 1 Schematic diagrams for metal shaped charge. (a) Detonated shaped charge showing slug and jet particulation. The liner cone is collapsed by a high explosive (HE). (b) Fluid jet model showing details of slug and jet formation from cone wall portions. The jet stretches and necks into particulates as a consequence of a velocity gradient. The jet velocity is shown as V_j while the slower-moving slug velocity is denoted V_s.

$> 0.6\ T_M$ (T_M is the melting point). The temperature issue, in connection with the detonating shaped charge, is still an unsettled question. Although it has been shown by flash X-ray diffraction that the elongating jet, even for light and low melting metals such as aluminium, remains crystalline (or polycrystalline), and is therefore a solid-state flow process [6, 7], there are no accurate measurements of temperatures. Zernow and Lowry [8] have estimated temperatures in copper jets to exceed about $0.7\ T_M$, but in the case of tantalum shaped charges [3, 5], the jet temperature would have to exceed 2000 °C at $0.7\ T_M$. At $\sim 0.7\ T_M$, the elongating jet represents high strain and strain rate hot working which is certainly conducive to dynamic recovery and recrystallization. However, even at low temperatures, microstructure evolution in extreme plastic flow can involve grain partitioning which can resemble recrystallized grains as a result of cell block and dense dislocation wall (or boundary) formation; characteristic of low-energy dislocation structures (LEDS) [9–11]. These features have recently been discussed in connection with explosively formed tantalum penetrators where strains are non-uniform and considerably lower than in the shaped charge [12].

In this investigation, we were interested in examining the effects that extremely small grain sizes in the starting liner cone would have on the residual (recovered) jet fragment microstructure, especially grain size. In addition, we were interested in examining these effects in a number of different metals, and comparing the variations in end-point microstructures observed. The observations included copper, molybdenum, and tantalum using both optical metallography and transmission electron microscopy (TEM).

2. Experimental procedure

We were particularly concerned in this study with the development of very small, starting grain-size metal liners so that we could compare the end-point (jet and slug) microstructure variations with the starting liner grain sizes. To achieve this, we utilized cones processed by sputtering, since this allowed not only for custom fabrication upon an appropriate cone form, but also grain size control not available through thermo-mechanical processing [13]. In addition, several forging schedules were developed to produce standard copper cones having grain sizes in the smallest range (10–15 μm) investigated previously by Duffy and Golaski [2]. However, unlike the standard 81-mm diameter cones of Duffy and Golaski [2], the cones produced for this study were smaller, speciality cones having wall thicknesses of about 1.5 mm, and a cone angle (α) of 60°.

Two different forged copper cones were produced in this study. These were compared with two different sputtered copper cone grain sizes which were microstructurally very different. In addition two different, sputtered molybdenum cones were produced for comparison with the sputtered copper (liner) cones. In addition, we compared the forged and sputtered copper cones with a larger grain size ($\sim$ 35 μm) copper forged cone from a previous study along with an equivalent size, equiaxed tantalum forged liner and a heavily deformed starting tantalum liner.

As in previous studies, the metal liners were detonated into a long (20 m) recovery tube filled with shaving cream and polystyrene sheets to facilitate the retrieval of the shaped charge component jet fragments and slugs [3]. The recovered jet fragments were usually too small for producing 3-mm discs for TEM, and the recovered jet fragments were built up by electroplating copper [3]. This electroplating process actually worked very well not only for the copper fragments, but also for the molybdenum and tantalum fragments as illustrated in Fig. 2.

Because we were primarily concerned in this study with a comparison of starting liner microstructures with the recovered jet fragment microstructures, samples were prepared from the inner 20% of the liner thickness as illustrated schematically in Fig. 2a. Fig. 2b–d also shows the build-up and sectioning of the recovered jet fragments as described above. Both transverse and longitudinal jet fragment sections were normally prepared which were first observed by optical metallography and then 3-mm discs were punched and electropolished to electron transparency for observations by TEM (Fig. 2d). A Hitachi H-8000 STEM operated at 200 kV in the conventional TEM mode was used for the electron microscope observations.

Table I lists the polishing and electropolishing solutions for optical metallography and electron microscopy respectively for the three metals examined in this investigation. The concentrations and conditions were often altered slightly as the microstructures varied significantly between the different liner metals and recovered shaped charge components.

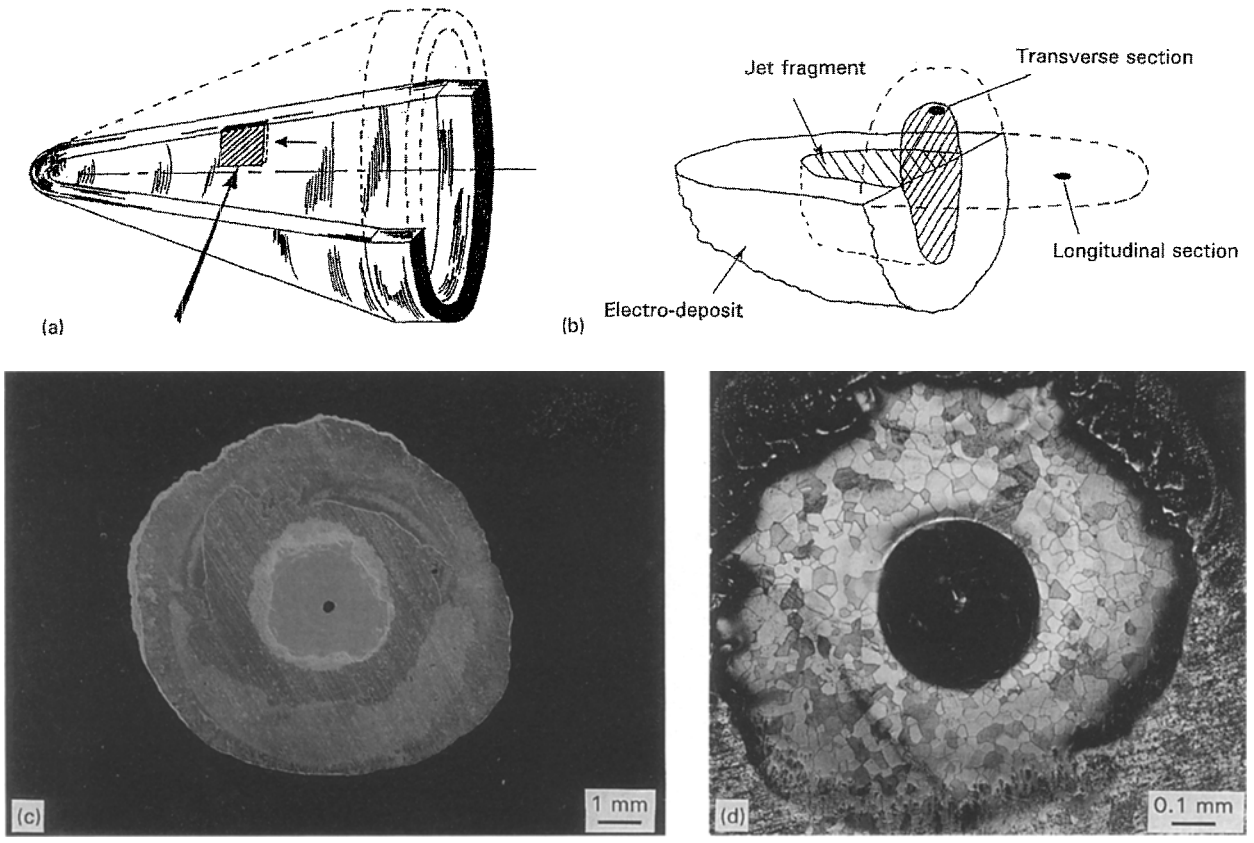

Figure 2 Specimen preparation from shaped charge components. (a) Schematic diagram showing inner liner wall sample location for viewing optical and TEM samples. (b) Schematic view of recovered jet fragment build up by copper electrodeposition and longitudinal and transverse section views. (c) SEM views of TEM jet specimen cross-section specimens of tantalum. Image to right is enlarged view near electron transparent region (d).

TABLE I Optical metallographic and electron microscopic etchants and electropolishing solutions for experimental samples[a]

Sample material	Etchant composition (Optical)	Electropolishing solution (TEM)
Copper	2 g $K(CrO_3)_2$ 100 ml H_2O 8 ml H_2SO_4 4 ml saturated NaCl solution rinse in deionized H_2O then acetone	500 ml ethanol 100 ml propanol 4 ml Struers' Vogels Sparbieze 10 g urea at − 10 °C; electropolish at 3–8 V
Molybdenum	Murakami's reagent (modified) 15 g K_3 $Fe(CN)_6$ 2 g NaOH 100 ml H_2O swab surface 10–20 s	3.5 ml H_2SO_4 200 ml H_2O 1275 ml methanol at 25 °C; 40 V, 0.6 A careful adjustment of flow rate
Tantalum	ASTM 66 etchant (modified) 4 parts HCl plus 2 parts HNO_3 plus 8 parts HF at 0 °C in nalgene beaker	90 ml HF 270 ml H_2SO_4 300 ml glycerol 1500 ml methanol at − 10 °C; electropolish at 3–8 V

[a] TEM samples were prepared as 3-mm discs in a Struers Tenupol 3 jet polisher. TEM discs were normally punched and dimpled from thin sections ground and polished to 20–40 μm thickness.

3. Results and discussion

Through thermo-mechanical treatment of forged metal liners and manipulation of sputtering parameters, it was possible to produce significant variations in the starting liner grain sizes from 0.1 to 35 μm on average; with variations about the mean grain sizes which produced an overall spread of less than 0.05 μm to approximately 60 μm. Table II illustrates the starting (average) grain sizes for each of the experimental metals included in this investigation along with their densities and melting temperatures: copper (FCC), molybdenum (BCC) and tantalum (BCC). These metals represent a significant density range as well as melting temperature (Table II).

TABLE II Comparison of starting liner grain sizes

Liner metal	Initial grain size D_o (μm)[a]	Density (g cm^{-3})	Melting temperature T_M(°C)
Forged Cu (1)	35	8.96	1083
Forged Cu (2)	15	8.96	1083
Sputtered Cu (1)	1	8.96	1083
Sputtered Cu (2)	0.1	8.96	1083
Sputtered Mo (1)	0.3	10.22	2610
Sputtered Mo (2)	0.5	10.22	2610
Forged Ta (1)	35	16.6	3010
Forged Ta (2)	35[b]	16.6	3010

[a] Grain size measurements were made by averaging individual grain maximum and minimum dimensions and then averaging these averages for a minimum of 100 grains in each sampling.
[b] Heavily deformed and non-equiaxed grain structure.

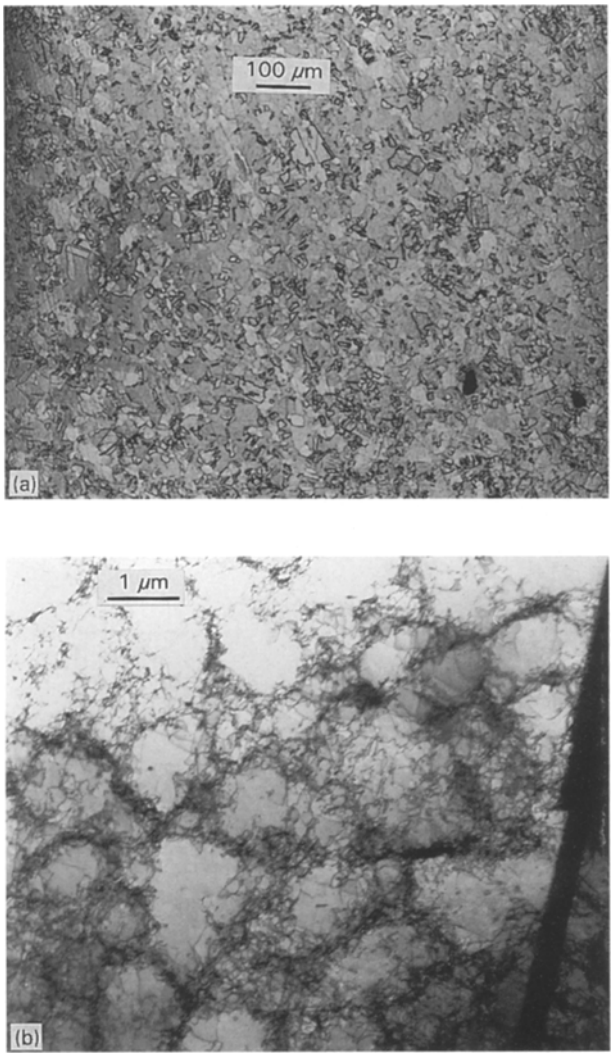

Figure 3 (a) Forged Cu (2) liner through-thickness microstructure. (b) TEM image of dislocation cell structure typical in recovered jet fragments corresponding to (a). This microstructure is often the same in the forged liner as well.

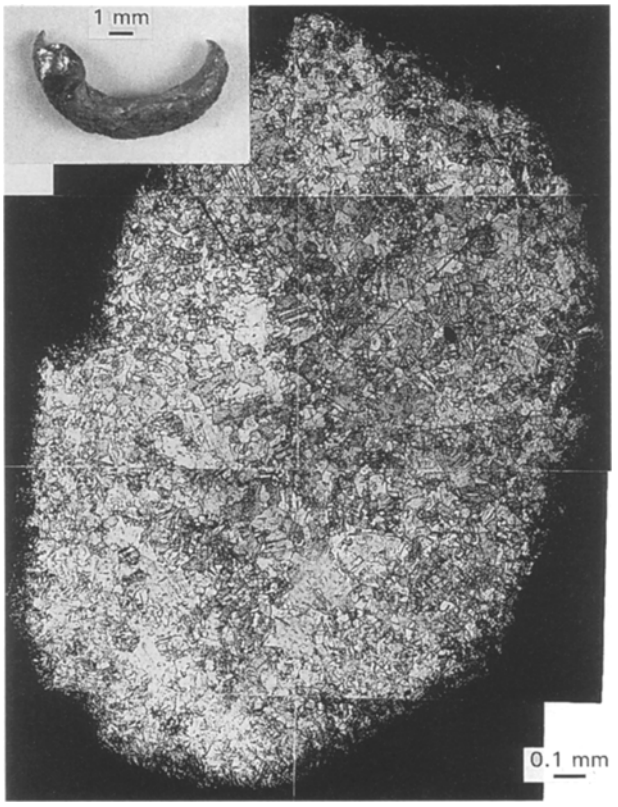

Figure 4 Cross-section (transverse) view of recovered jet fragment (insert) corresponding to Fig. 3a.

3.1. Copper shaped charges

Fig. 3 illustrates the equiaxed, twinned microstructure specific to the forged Cu (2) liner cone. Fig. 3a shows an optical metallographic view through the entire cone thickness (and at 90° to the in-plane schematic of Fig. 2a). This view is also typical for all forged Cu liner microstructures including the in-plane views illustrated in previous work [3, 5]. The TEM image of dislocation cells shown in Fig. 3b is also typical of the liner substructures although it illustrates the substructure typical of the recovered jet cross-sections for Cu (2) samples. This sample (Fig. 3b) corresponds to the cross-section for the jet fragment shown in Fig. 4. Taking into account the magnification difference between Fig. 4 and Fig. 3a it can be observed that there is a reduction in the recovered jet grain size from 15 μm in the starting liner (Table II) to an average of 8 μm. This is a much smaller reduction than in the forged Cu (1) sample. In addition, the jet cross-section exhibited a more uniform structure in Fig. 4 as compared to Cu (1) which often exhibited a series of concentric and varying grain sizes. This feature was

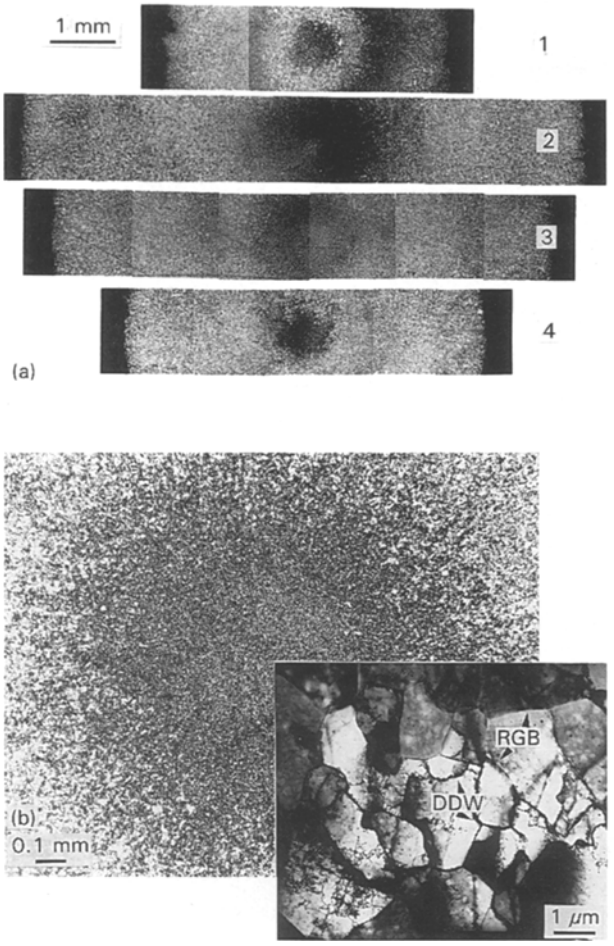

Figure 5 (a) Series of transverse or cross-sectional views for Cu (1) slug. Concentric zones exhibit varying grain size regimes with the smallest grains in the slug centre shown in (b) and in TEM image insert in (b). The region shown in (b) corresponds to position 2 in (a). Positions 1–4 in (a) correspond to the slug tip at 1 and moving away from the tip in succession to 4. Dense dislocation walls are denoted DDW and regular grain (or sub-grain) boundaries denoted RGB in insert in (b).

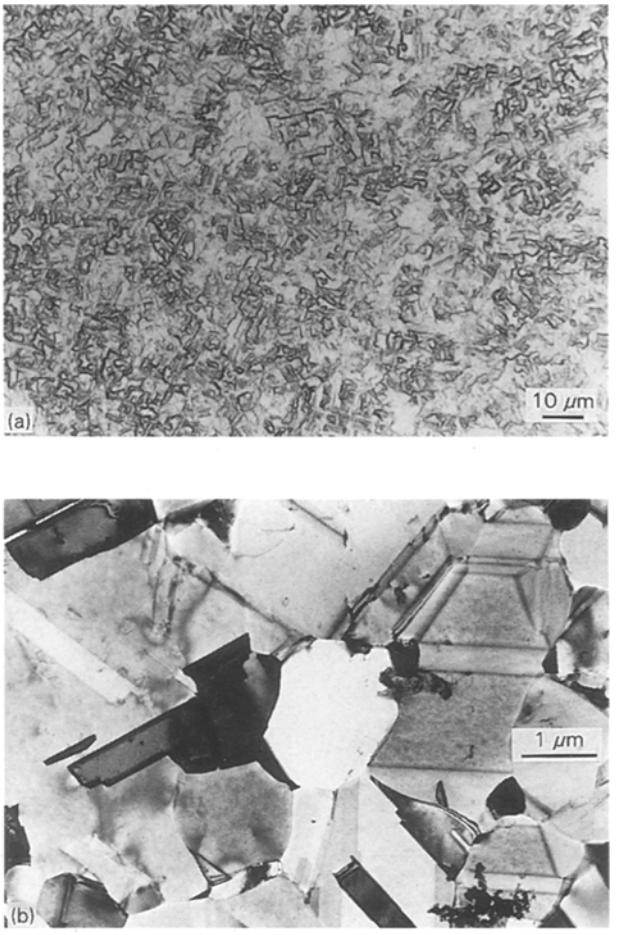

Figure 6 Sputtered Cu (1) liner microstructure. (a) In-plane liner optical micrograph showing heavily twinned grains. (b) TEM image shows annealing and growth twins producing a kind of equiaxed microstructure.

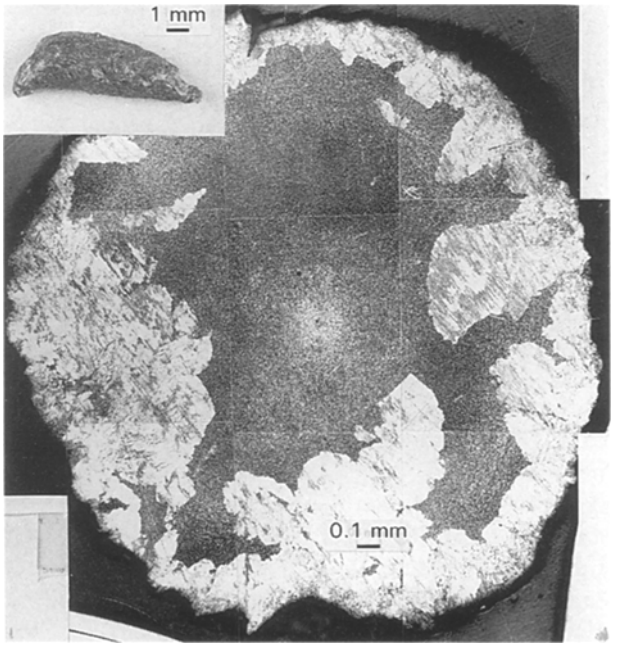

Figure 7 Optical metallographic view of recovered, sputtered Cu (1) jet fragment (insert) cross-section.

also characteristic of the slug as illustrated in Fig. 5. The slug centre in Fig. 5 exhibited an extremely small sub-grain microstructure, shown in the insert to Fig. 5b, and composed of dense dislocation walls [9] as well as regular grain boundaries separating crystallographically different subgrains having an average grain size of about 2 μm; a factor of about 15 difference between the starting liner grain size and the smallest, recovered slug grain size. This was also typical of recovered jet fragments for Cu (1) samples. One of the other significant microstructural differences between the microstructure near the slug centre in Fig. 5b, and the starting liner microstructure, is the absence of annealing twins and twin faults which is a clear indication of dynamic recrystallization.

This microstructural feature was one of the more significant observations in the cross-sections of recovered jet fragments for the sputtered copper liners (1 and 2 in Table II). In addition, the jet fragment microstructures exhibited the kind of crystallization (or recrystallization) behaviour typical of solidification from the melt where annealing twins are absent. These features are shown in Figs 6–8. Fig. 6 shows the initial sputtered Cu (1) liner microstructures to be characterized by very small equiaxed and twinned grains while Fig. 7 shows the overall recovered jet fragment cross-section for comparison with Fig. 4.

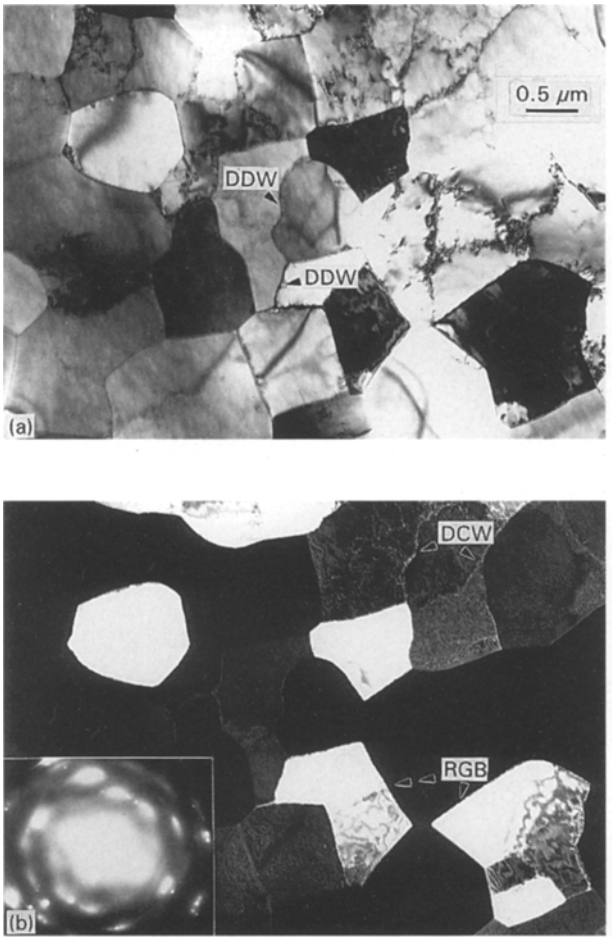

Figure 8 Bright (a) and dark-field (b) TEM images typical of central jet microstructure in Fig. 7. Equiaxed grains are devoid of twin boundaries. The dark-field image in (b) corresponds to reflection shown circled in selected-area electron diffraction pattern insert. Boundary types are noted DDW, RGB, or DCW.

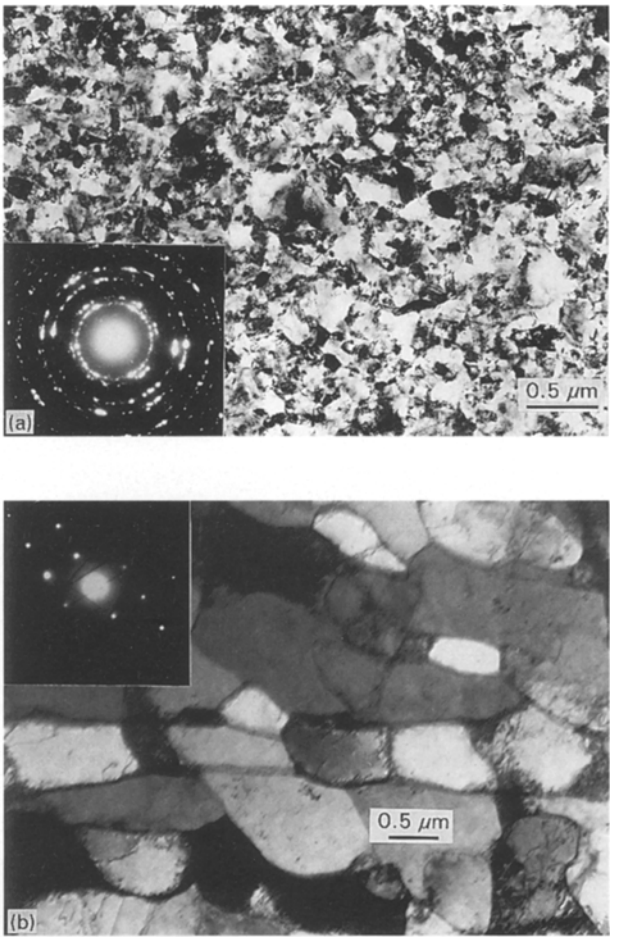

Figure 9 TEM bright-field images of sputtered Cu (2) liner (a) and recovered jet centre microstructure (b). Very fine growth twins are interspersed in the microstructure in (a) (SAD insert). The corresponding jet cross-section in (b) was similar to Fig. 7. Large crystalline areas contained equiaxed cells or sub-grains often exhibiting very low misorientations illustrated in (b) (SAD insert).

Fig. 7 shows a very small central region similar to the copper slug microstructure in Fig. 5b. Fig. 8 shows a microstructure similar to that in the insert of Fig. 5b for the recovered, sputtered Cu (1) jet in Fig. 7 which shows the absence of twins and well-formed, equiaxed sub-grains for comparison with the starting liner microstructure in Fig. 6b. This microstructure is characteristic of many of the large "grain" zones in Fig. 7 where there are no annealing or growth twins. However, as illustrated in the dark-field TEM image of Fig. 8b, many of the sub-grains are crystallographically distinct from neighbouring sub-grains, and misorientations of boundaries separating apparently common crystallographic orientations range from about 9 to 16°. Many of the residual jet microstructures for sputtered Cu (1) samples exhibited a wide range of boundary characteristics shown typically in Fig. 8. These include dislocation cell walls (DCWs), dense dislocation walls (DDWs), and regular grain boundaries (RGBs). As shown on comparing the corresponding bright and dark-field TEM images in Fig. 8, sub-grain or grain regions which are bounded by RGBs usually exhibit strong diffraction contrast conditions throughout the grain, while there is no contrast reversal region exhibiting dislocation cells and cell walls; having very small misorientation of 1–2° (Fig. 8b upper right region for example). An interesting feature on comparing Fig. 6b and Fig. 8a is the fact that the average grain or sub-grain size is little changed since the average grain size in Fig. 8 is about 1.5 μm in contrast to 1 μm in Fig. 6. It is apparent on comparing forged Cu (1) and (2) and sputtered Cu (1) that as the starting liner grain size is reduced, there is apparently a smaller difference between the starting liner grain size and the average recovered jet and slug grain size; the ending shaped charge grain size, which we will designate D_s. This feature is even more dramatic for the sputtered Cu (2) shaped charge samples where the starting liner grain size was an order of magnitude smaller, on average, than that of sputtered Cu (1) (Table II), while the recovered jet fragments exhibited microstructures similar to Fig. 7. However, as illustrated on comparing Fig. 9a and b, the residual sub-grain structure is dominated by cell-like microstructures or DCWs. These cells or sub-grains, having small misorientations (1–4°), exhibit an equiaxed microstructure also devoid of growth or annealing twins; and average sizes of 1.5 μm. This size is commensurate with the more established subgrain size in Fig. 8. It is of interest to compare the dramatically reduced sputtered grain structure in Fig. 6b with that in Fig. 9a which also

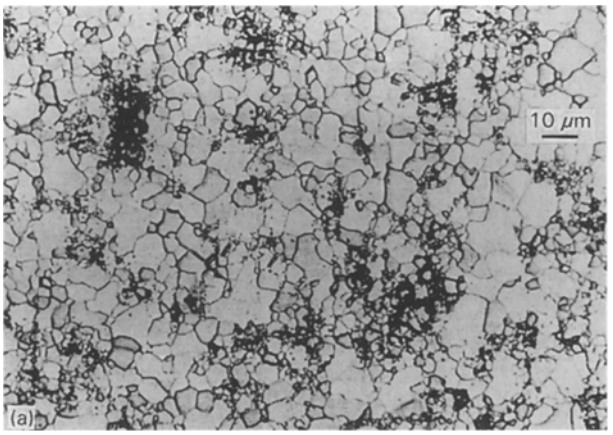

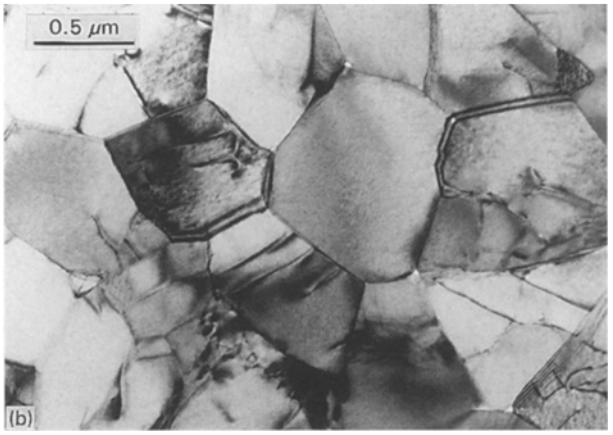

Figure 10 Sputtered Mo (2) starting liner microstructure observed in the plane of the liner (Fig. 2a). (a) Optical metallographic image. (b) TEM image showing equiaxed grain structure.

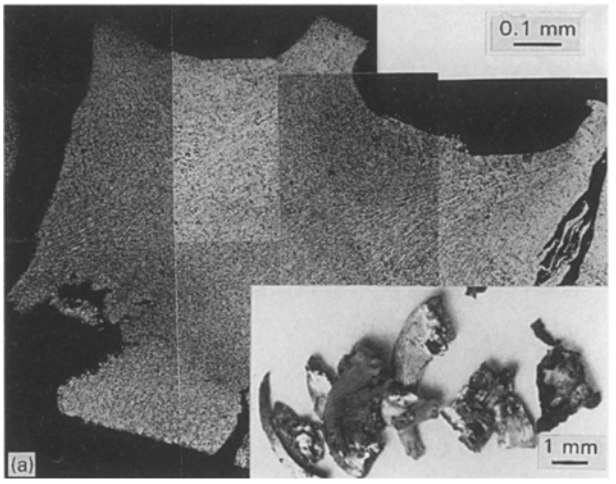

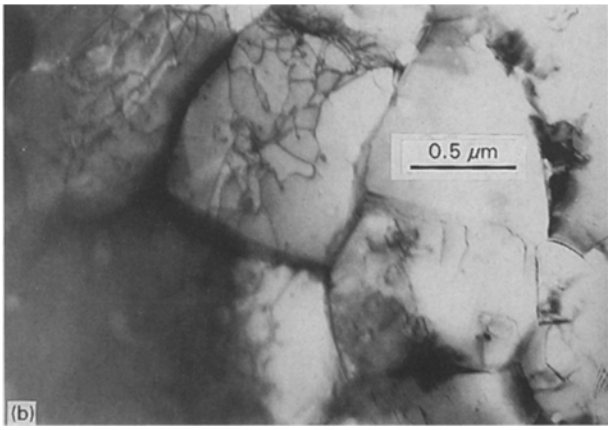

Figure 11 Recovered Mo (2) jet fragment microstructure. (a) Irregular fragments (insert) exhibit "flow" patterns and very small grain size. (b) TEM image showing equiaxed grain structure similar to the starting liner.

exhibits a high density of twinning as a consequence of sputter-growth accidents in building the starting liner.

Of course the microstructural features could occur, or evolve, as a consequence of low energy dislocation structures (LEDS) evolution [9–11], but the detonating shaped charge is a hot deformation process as a consequence of the adiabatic product, $(\varepsilon \cdot \dot{\varepsilon})$, which approaches $10^8\ s^{-1}$ in contrast to low temperature plastic deformation processes involving rolling or wire drawing at low rates where this product may vary from 10 to $10^4\ s^{-1}$. Consequently, it is certainly compelling to assume, as previously asserted [3–5], that dynamic recovery and recrystallization play a significant role in the deforming shaped charge.

3.2. Molybdenum shaped charges

The sputtered molybdenum shaped charge liners, like those for sputtered copper, were characterized by very small starting grain sizes (Table II). Like the sputtered copper, the sputtered molybdenum shaped charges exhibited very restricted grain size variations between the starting and ending liners and jet fragments respectively. These features are illustrated on comparing the corresponding microstructures for sputtered Mo (2) samples in Figs 10 and 11. The equiaxed grain structure in the starting Mo (2) liner is, like the sputtered Cu samples, actually larger in the recovered, ending jet fragments than the starting liners since the average Mo (1) and Mo (2) jet fragment grain sizes are about 1 μm. Unlike the sputtered copper samples in Figs 8 and 9, the residual, sputtered Mo jet fragment samples consisted of fine grains characterized by RGBs; with a higher residual dislocation density than the starting liner grain structure. On comparing the sputtered Cu and Mo shaped charges, there is a consistent residual, or steady-state grain size, D_s of about 1 μm [14–16]. This is larger than the starting liner grain size, D_o; and $D_o/D_s \leqslant 1$.

It should also be noted in Fig. 11, in contrast to copper, that the Mo jet fragments are irregular and not necked. Both Mo samples (1 and 2) exhibited this apparently irregular fragmentation.

3.3. Tantalum shaped charges

In contrast to the sputtered Cu and Mo shaped charges, we re-examined several forged Ta shaped charges. In forged Ta (1) specimens, the starting liner was characterized by very equiaxed, symmetrical grains having a mean size of about 35 μm (Table II). The detonation of these liners produced jet fragments often exhibiting a relatively uniform cross-section, while the residual slug exhibited a very systematic,

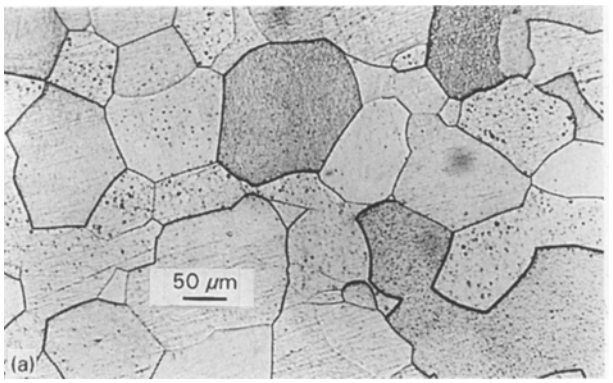

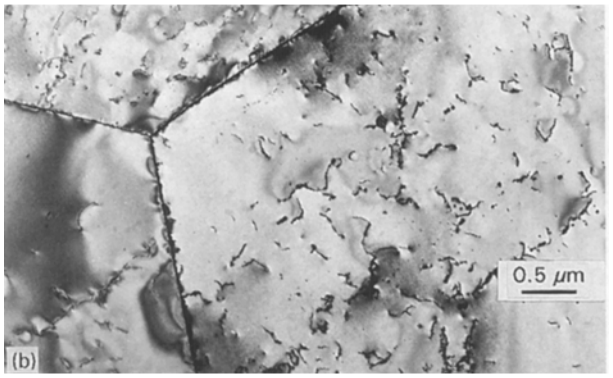

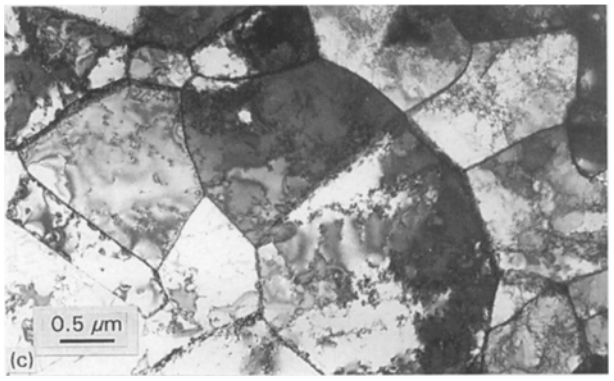

Figure 12 Ta (1) microstructures. (a) Starting liner in-plane grain structure. (b) TEM image typical of grain structure in (a). (c) TEM image of recovered jet fragment centre microstructure corresponding to (a).

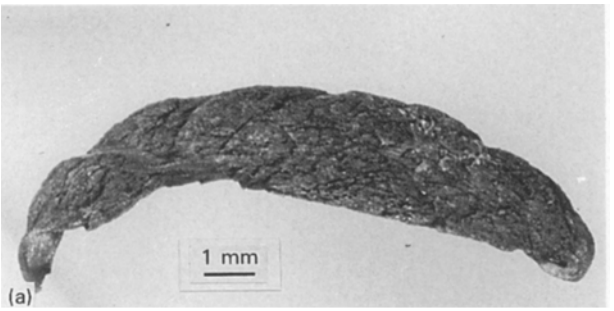

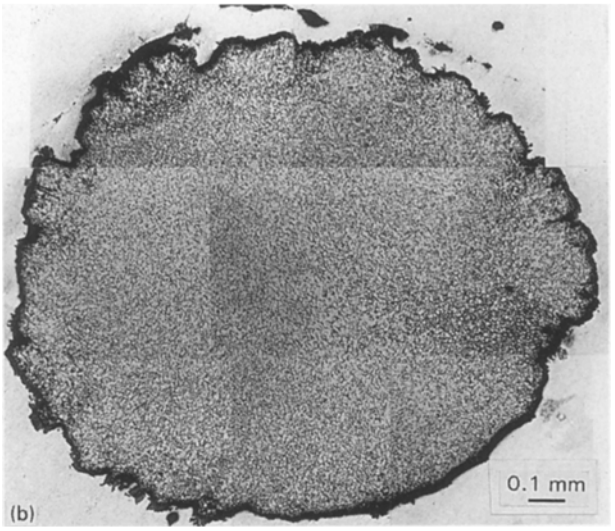

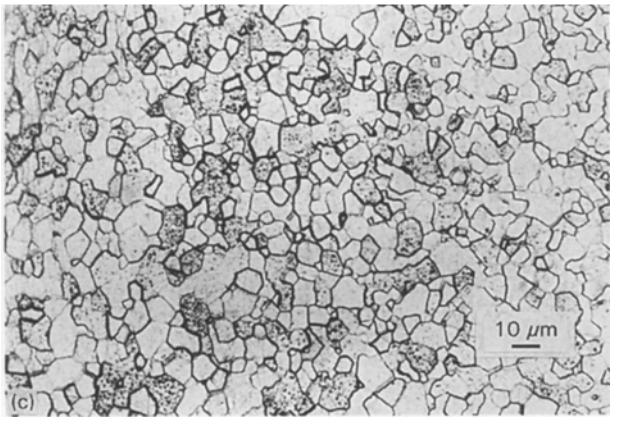

Figure 13 Recovered Ta jet fragment (a) showing essentially uniform cross-section microstructure (b) similar to forged copper (Fig. 4). (c) Shows magnified view of equiaxed grain structure.

concentric series of microstructural zones similar to those illustrated for forged Cu in Fig. 5a. These features are illustrated in Figs 12 and 13 which compare the liner and jet fragment microstructures. Here the residual, central jet grain structure is reduced from the liner grain size by about 10^{-2} (to about 0.35 μm; compare Fig. 12a and c).

In contrast to the relatively uniform jet fragment cross-section microstructure, the corresponding slug microstructure exhibits rather systematic, evolutionary features from the slug centre to the perimeter, as shown in Figs 14 and 15 in comparison with Figs 12 and 13. Figs 14 and 15 show the connection between dynamically recovered and recrystallized regions as well as the evolutionary microstructural features characteristic of low-temperature deformation LEDS. Another interesting feature illustrated in Fig. 14 is the corresponding microhardness changes from the slug perimeter to the centre in contrast to the starting Ta (1) liner microhardness of VHN using a 100 gf load standard. This is a particularly interesting phenomenon since the contrast in grain size from the liner to the slug centre is 10^2 (35–0.35 μm) while the corresponding (average) microhardness from the liner to the slug centre is observed to be 109 VHN to 127 VHN respectively. The maximum slug microhardness is observed to be 180 VHN (Fig. 14). The considerable softening in the slug centre is indicative of the work softening associated with classical dynamic recrystallization [17] as the dislocation density is reduced (Fig. 15a). However the higher hardness in the slug

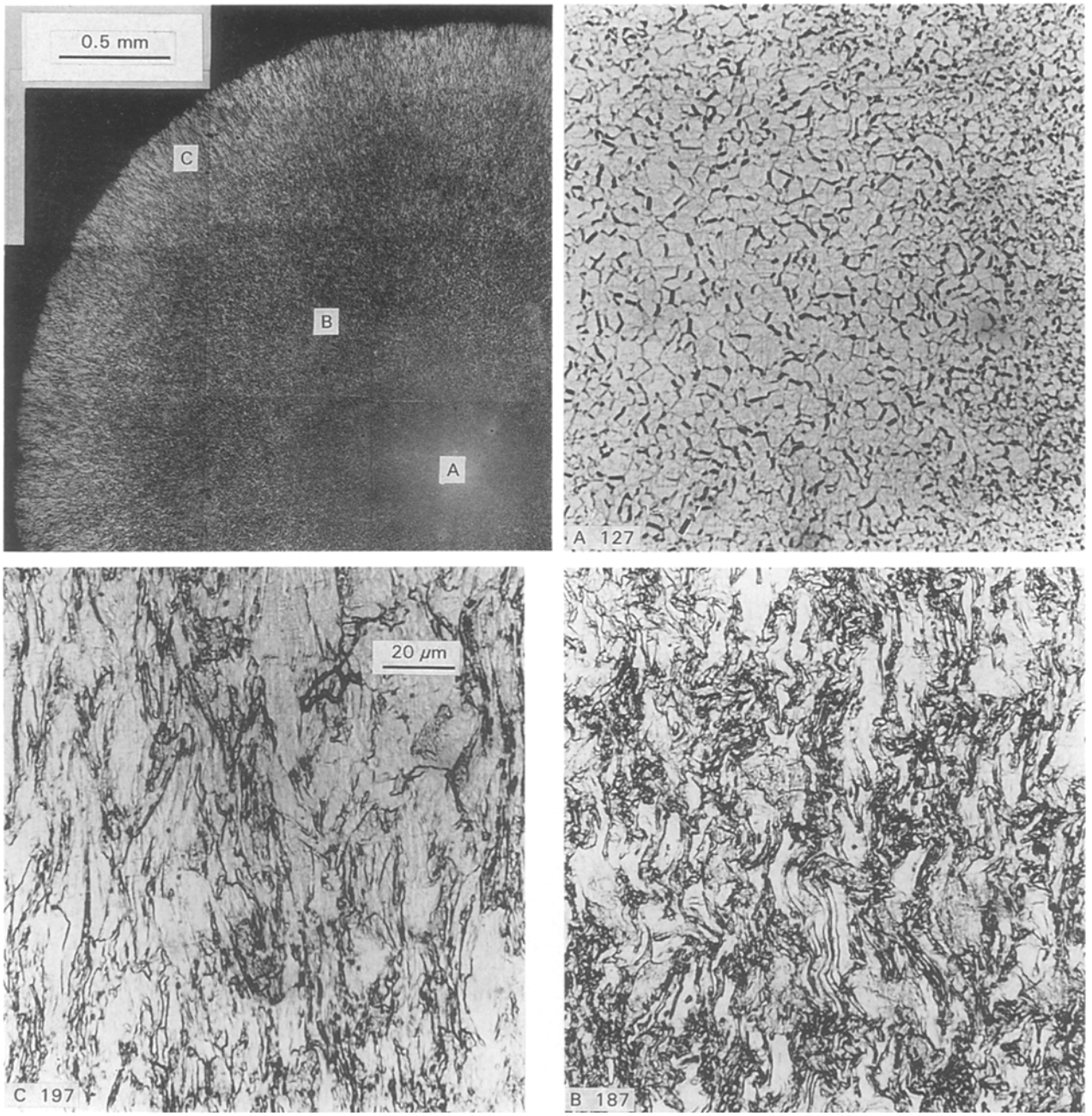

Figure 14 Recovered Ta slug cross-section views. The microstructure varies somewhat systematically from the slug centre to its perimeter and the corresponding microhardness is indicated for the zones indicated A, B, C. Microhardness values are in VHN (100 gf load).

centre in contrast to the starting liner can be attributed to the significantly smaller grain size in the slug centre ($\sim 10^2$ smaller) in contrast to the liner.

Finally, in the case of a heavily deformed, forged Ta liner (Ta (2)), it has been observed that in contrast to the equiaxed and well-annealed starting liner (Ta (2)) the residual (or recovered) jet fragments and slug exhibit essentially the same microstructural features, but the steady-state grain size average is about 0.5 μm in contrast to 0.35 μm for Ta (1) samples. These features are contrasted with the equiaxed grain structure in Ta (1) as illustrated on comparing Fig. 16 with Fig. 12, and Fig. 17 with Fig. 15; taking account of the differences in magnification between Fig. 15(a) and Fig. 17. Not only is the grain size larger in Fig. 17 but the dislocation density within the grains larger than in Fig. 15(a), for example. Fig. 17 also illustrates the high density of dislocation loops which are a characteristic of the slug centre as well as the jet centres; indicative of the propensity for dislocation climb at the elevated temperatures which are assumed to be associated with the detonating Ta shaped charge.

3.4. Steady-state grain size development and volume stored energy

The fact that the sputtered, very small-grained Cu and Mo starting liners produced a smaller value of D_o/D_s in contrast to larger forged liner grain sizes and that D_o/D_s is smaller in the heavily deformed Ta (2) sample than the equiaxed, annealed Ta (1) sample seems to illustrate a trend of microstructural influence and in the evolution of microstructures, including dynamic recrystallization phenomena in the recovered, end-point components. This effect, illustrated in the comparative data for all of the experimental samples plotted in Fig. 18, would seem to be associated with the stored energy differences and its influence on

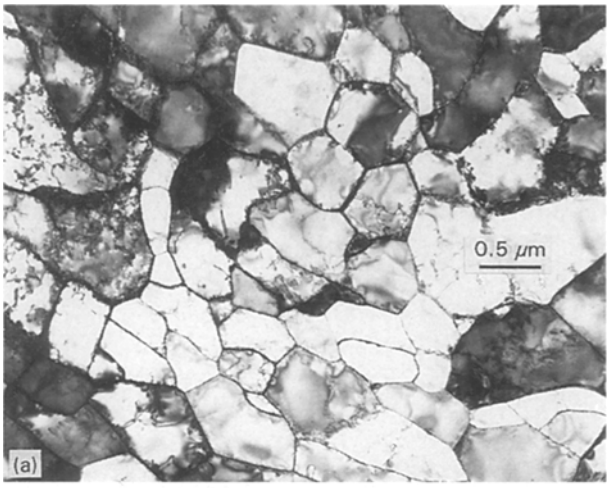

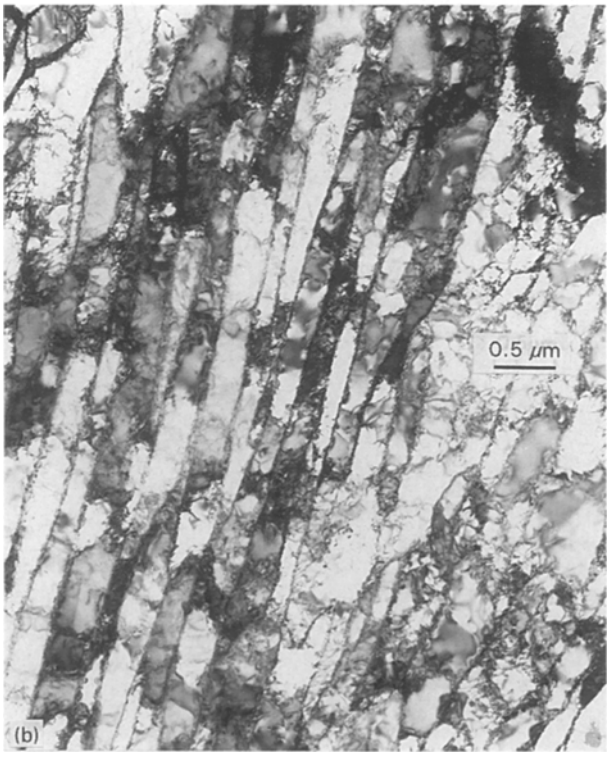

Figure 15 TEM images corresponding to zones A and B in Fig. 14: Ta slug.

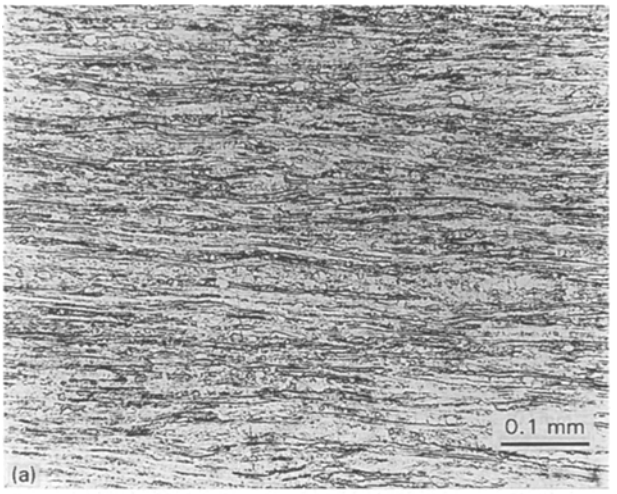

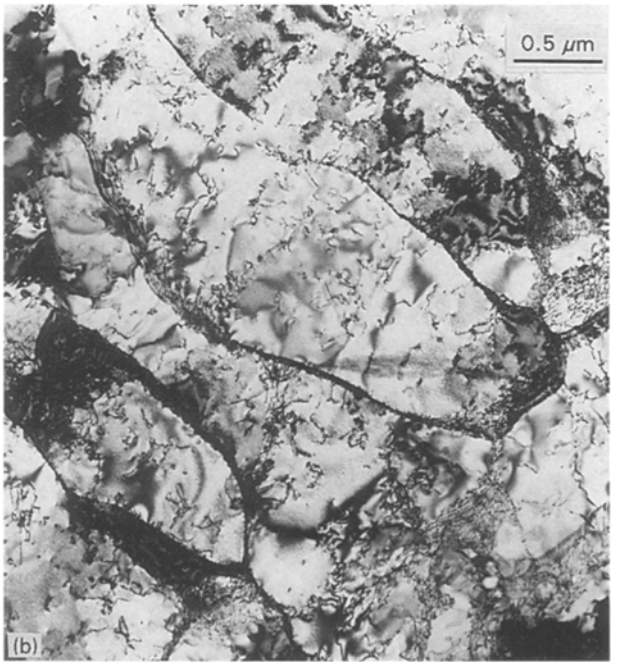

Figure 16 Forged and deformed Ta (2) liner microstructure. (a) Optical metallographic image. (b) TEM image of (a) showing a variety of boundary and cell-wall structures as well as a significant dislocation density distributed somewhat uniformly.

LEDS evolution in a general context, and dynamic recovery and recrystallization specific to hot deformation characteristic of the detonating shaped charge. That is, the total volume stored energy might be expressed by a grain boundary contribution: $(\Gamma\gamma_{gb}/D_o)$; where Γ is a constant which includes a geometrical factor characteristic of the grain boundary, γ_{gb} is the specific grain boundary free energy (per unit area of interface), and D_o is the starting grain size (in the liner; Table II). An additional term would include the uniform stored energy due to the deformation-induced defects, and defects, especially dislocations, present at the outset in the liner, and generally expressed in some form like $(\alpha Gb^2\rho)$; where α is a constant, G is the shear modulus, b is the dislocation Burger's vector, and ρ is the dislocation density (cm^{-2}). Consequently, the available energy initially is given by

$$E_o = (\Gamma\gamma_{gb}/D_o) + (\alpha Gb^2\rho) \quad (1)$$

and of course this energy is continuously (or discontinuously) altered as the shaped charge deformation continues.

Consequently, as the liner volume stored energy is increased dramatically through the development of extremely small starting grain sizes and/or initial heavy deformation creating dense dislocation microstructures within these small grains (Fig. 16), the intrinsic driving force for plastic flow and energy minimization will increase substantially. At sufficiently small starting liner grain sizes, (D_o) the steady-state grain size in the elongating jet will approach some constant value. This value appears from Fig. 18 to be around 1 μm. The fact that Fig. 18 demonstrates a relationship between the starting liner grain size and the ratio D_o/D_s is indicative of the role that microstructure in general, and volumetric stored energy in particular, plays in the deforming shaped charge.

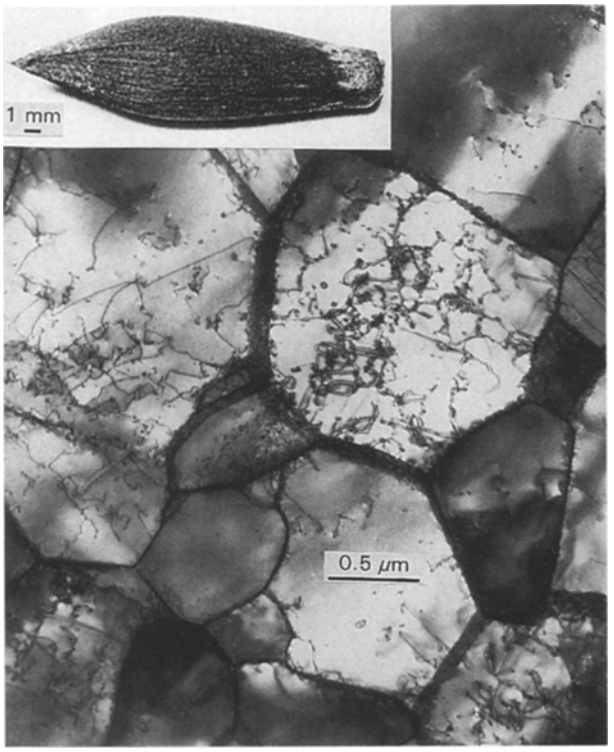

Figure 17 TEM bright-field image showing magnified view of slug centre corresponding to Ta (2) sample in Fig. 16. The corresponding, recovered slug is shown in the insert. The cross-section for TEM was cut from the region of maximum slug diameter (insert). Note the regular grain boundary and other boundary microstructures.

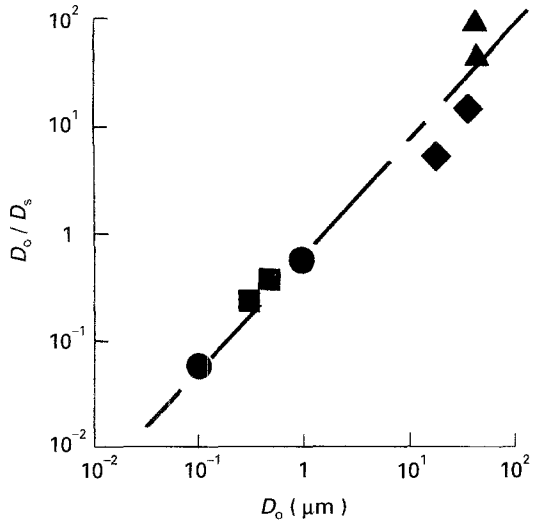

Figure 18 Plot of beginning liner grain size (D_o) versus D_o/D_s (D_s is the ending jet fragment centre grain/sub-grain size). ● Cu (sp); ■ Mo (sp); ◆ Cu (for); ▲ Ta (for).

While the evidence for dynamic recrystallization in the shaped charge regime seems overwhelming, it must be recognized that very little is known about dynamic recrystallization at high strain rates. In addition, the role played by dynamic recrystallization cannot be independently assessed, and LEDS theory provides for microstructural similarities even for low temperature deformation.

In the case of LEDS theory, there are three important principles: the second law of thermodynamics is a driving force for establishing a specific microstructure in response to a particular deformation, the development and evolution of LEDS is glide-dominated for low temperature deformation, and the microstructure itself (that is the specific nature of the microstructure) is a representation of the degree of deformation [9–11]. There is, of course, ample evidence for the variety and evolutionary features of LEDS as demonstrated on comparing Figs 3b, 5b, 8, 9b, 11b, 12c, 14–17. These microstructures, although for different metals and crystal structures (FCC, BCC) represent a wide range of LEDS. In addition there is a gradual increase in boundary misorientation of the dislocation cell structures and at sufficiently large misorientations the sub-boundary and grain boundary structures are indistinguishable; consistent with the features of dynamic recrystallization described by Derby [18]. However, since the shaped charge is a plastic flow regime involving high temperature, the intervention of dislocation climb in the microstructure development provides an important if not dominant feature. Consequently, dynamic recovery in the classical sense may indeed play a significant role in the deformation process, and dynamic recrystallization is a very important mechanism in shaped charge deformation. It is also apparent that jet and slug formation involve different plastic flow processes, and the recovered jet microstructures are apparently dominated by dynamic recrystallization, while only the slug centre is predominantly a region exhibiting dynamic recrystallization.

While it is certainly clear that microstructure plays an important role in the deformation of the shaped charge, the specific nature of microstructural effects are unknown except to influence the steady-state grain size. In the absence of shaped charge jet penetration data, it is difficult to speculate on the effect of microstructure and microstructure evolution on the shaped charge performance, but it is apparent that a small liner grain size and heavy deformation are desirable since this ensures a larger volumetric stored energy which drives the steady-state grain size to a small value.

4. Conclusions

The beginning microstructures (including grain sizes) for forged and sputtered metal shaped charge liners (forged and sputtered Cu (FCC), sputtered Mo (BCC) and forged Ta (BCC)) have been compared with corresponding, recovered (ending) jet fragments (Cu, Mo, and Ta) and slugs (Cu, Ta). A wide range of microstructures including dislocation cells (including tilt and twist boundaries), geometrically necessary boundaries (including dense dislocation walls and regular grain boundaries and sub-boundaries) consistent with low-energy dislocation structure (LEDS) types have been observed, and evolutionary features of these microstructures have also been observed in Ta slugs. The ending jet microstructures are dominated by dynamic recrystallization while the slug exhibits dynamic recrystallization in the centre, dynamic recovery, and related deformation microstructures, including dislocation cells. The slug centre in Ta

exhibited significant softening in contrast to the outer slug regions. There was a systematic relationship between the starting (average) grain size in the liner (D_o) and the ratio of starting/ending (jet) grain size (D_o/D_s). In addition, the shaped charge ending grain structure is influenced by not only the starting grain size but also the degree of deformation (or dislocation density) which accounts for the total volumetric stored energy. It appears that high volumetric stored energy in the starting liner is largely responsible for jet stability and enhanced penetration in the shaped charge, but this is speculative in the absence of corresponding jet penetration data.

Acknowledgements

This research was supported in part by ZTS Prime Contract DAA H01-92-C-R044 (Department of the Army) and subcontract ZSC-93-001 (3155). The research was also supported by a Mr and Mrs MacIntosh Murchison Chair (L.E.M.) and a Patricia Harris Roberts Fellowship (J.C.S.).

References

1. W. P. WALTERS and J. A. ZUKAS' "Fundamentals of shaped charges" (Wiley Interscience, New York, 1989).
2. M. L. DUFFY and S. K. GOLASKI, "Effect of liner grain size on shaped charge jet performance and characteristics", Technical Report BRL-TR-2800, U.S. Army Ballistic Research Laboratory, Aberdeen Proving Ground, MD, April, 1987.
3. A. C. GUREVITCH, L. E. MURR, H. K. SHIH, C.-S. NIOU, A. H. ADVANI, D. MANUEL, and L. ZERNOW, *Materials Characterization* **30** (1993) 201.
4. L. E. MURR, H. K. SHIH, C.-S. NIOU, and L. ZERNOW, *Scripta Metall. et Materialia* **29** (1993) 567.
5. L. E. MURR, H. K. SHIH and C.-S. NIOU, *Materials Characterization* **33** (1994) 65.
6. F. JAMET, "Investigation of shaped charge jets using flash X-ray diffraction", Eighth Symposium on Ballistics, Orlando, FL, October, 1984.
7. F. JAMET and R. CHARON, "A flash X-ray diffraction system for shaped charge jets analysis", Report (0211/86) Franco-German Research Institute, Saint-Louis, France, May, 1986.
8. L. ZERNOW and L. LOWRY, in "Shock-wave and high-strain-rate phenomena in materials", edited by M. A. Meyers, L. E. Murr, and K. P. Staudhammer (Marcel Dekker, New York, 1992) Ch. 46.
9. D. KUHLMANN-WILSDORF, *Phys. State Sol. (a)* **104** (1989) 1.
10. D. KUHLMANN-WILSDORF, *Materials Sci. Engr.* **A113** (1989) 1.
11. B. BAY, N. HANSEN, D. A. HUGHES, and D. KUHLMANN-WILSDORF, *Acta Metall. et Materialia* **40(2)** (1992) 205.
12. L. E. MURR, C.-S. NIOU, and C. FENG, *Scripta Metall. et Materialia* **31 (3)** (1994) 297.
13. D. MERZ, Battelle-Pacific Northwest Laboratory (PNC), private communication, 1993; sputtered liners utilized in this research programme were processed by D. Merz.
14. A. H. CHOKSHI and M. A. MEYERS, *Scripta Metall. et Materialia* **24** (1990) 605.
15. R. SANDSTROM and R. LAGNEBORG, *Acta Metall.* **23** (1975) 387.
16. B. DERBY and M. F. ASHBY, *Scripta Metall.* **21** (1987) 879.
17. T. SAKAI and J. J. JONAS, *Acta Metall.* **32** (1984) 189.
18. B. DERBY, *ibid.* **39(5)** (1991) 955.

Received 30 August
and accepted 10 October 1994